Applied Catalysis B: Environmental 96 (2010) 329–337

Contents lists available at ScienceDirect

Applied Catalysis B: Environmental

journal homepage: www.elsevier.com/locate/apcatb

Tuning operational conditions for efficient NO_x storage and reduction over a Pt–Ba/Al_2O_3 monolith catalyst

Beñat Pereda-Ayo[a], Divakar Duraiswami[a], Juan J. Delgado[b], Rubén López-Fonseca[a], José J. Calvino[b], Serafín Bernal[b], Juan R. González-Velasco[a,*]

[a] Departamento de Ingeniería Química, Facultad de Ciencia y Tecnología, Universidad del País Vasco/Euskal Herriko Unibertsitatea, Campus de Leioa, P.O. Box 644, ES-48080 Bilbao, Bizkaia, Spain
[b] Departamento de Ciencia de Materiales e Ingeniería Metalúrgica y Química Inorgánica, Facultad de Ciencias, Universidad de Cádiz, Campus Río San Pedro, ES-11510 Puerto Real, Cádiz, Spain

ARTICLE INFO

Article history:
Received 14 December 2009
Received in revised form 12 February 2010
Accepted 20 February 2010
Available online 1 March 2010

Keywords:
NSR
Efficiency
NO_x
Storage
Reduction
Lean-burn engines
Monolith
Platinum
Barium

ABSTRACT

A well-controlled homemade Pt–BaO/Al_2O_3 monolith catalyst has been used for tuning the operational conditions at which the NO_x storage and reduction (NSR) of the lean-burn engine exhaust gases is achieved more efficiently. The following operational conditions have been analyzed: the duration of the lean (storage) period, and the reductant (H_2) concentration and duration of the regeneration (rich) period. The storage pattern during the lean period is evaluated by the percentage of NO_x stored or NO_x trapping efficiency (η_T), and the performance during the rich period is evaluated by the NO_x reduction conversion (X_R) and the selectivity to nitrogen (S_{N_2}). These three response variables have been integrated into the single parameter that we have named integral NSR efficiency (ε_{NSR}) of the whole NSR process, which represents the percentage of N_2 produced at the reactor exit relative to the NO_x fed to the reactor. The proposed graphical map consists of a series of ε_{NSR}-isocurves and allows predicting the NSR efficiency for any combination of the three studied operational conditions (C_{H_2}, t_R, t_L). Such operational map shall also be useful to compare the global NSR behavior of commercial catalysts under real operating conditions.

1. Introduction

Diesel and lean-burn engines provide better fuel economy and produce lower CO_2 emissions compared to conventional Otto gasoline engines. However, the NO_x gas components in the lean (oxidizing) exhausts from diesel and lean-burn engines cannot be efficiently removed with the classical three-way catalyst under operating conditions with excess of oxygen in the exhaust gas. Among the available technologies under research, the NO_x storage-reduction (NSR) catalyst seems to be the most promising method to solve the problem [1–3].

Basically, an NSR catalyst consists of a cordierite monolith washcoated with a porous alumina on which an alkali or alkali-earth metal compound and a noble metal are deposited. The most common NSR catalyst formulation used is Pt–BaO/Al_2O_3. These catalysts work under alternating conditions of fuel lean (oxidizing) and fuel rich (reducing) environments. Under lean conditions, when oxygen is in excess, the platinum oxidizes NO to a mixture of NO and NO_2 (NO_x), which is adsorbed (stored) on Ba as various NO_x species (nitrate, nitrite). During the subsequent short period under rich conditions, when some reductant is injected, NO_x species are released and reduced to nitrogen on Pt [3]. The effectiveness of different types of reductants such as propylene, CO, H_2, and NH_3 has been compared by many researchers [4–8]. Hydrogen has been found to be the most effective reductant. Reaction of NO_x with H_2 can produce a complex mixture of N_2, NH_3 and N_2O, mainly dependent on temperature [4,7,8].

The last comprehensive review on this topic by Roy and Baiker [9] elucidates the importance of the material properties of the catalyst, such as chemical composition, structure, and morphology, and these properties are related with the mechanism and performance of the storage-reduction process (more than 370 references are included in [9]).

The chemistry and mechanism involved during lean and rich periods in the literature show overall similar common features. Most of these studies have focused on the NO_x storage process [8,10–12] but lately the reduction step [12–16] has received considerable attention. Nevertheless, there exist some divergent views and apparently opposite conclusions, which may be due to the partly different experimental conditions used by the various

* Corresponding author. Tel.: +34 94 601 26 81; fax: +34 94 464 85 00.
E-mail address: juanra.gonzalezvelasco@ehu.es (J.R. González-Velasco).

0926-3373/$ – see front matter © 2010 Elsevier B.V. All rights reserved.
doi:10.1016/j.apcatb.2010.02.029

Nomenclature

C_{H_2}	hydrogen concentration fed during the rich period, %
F^0_{NO}	NO molar flow at the reactor inlet, mol min^{-1}
F_{NO_x}	NO_x molar flow at the outlet reactor, mol min^{-1}
NO^{in}	amount of NO fed, μmol
NO_x^{out}	amount of NO_x leaving the reactor, μmol
NO_x^{stored}	total amount of NO_x stored, μmol
S_{NH_3}	cycle-averaged selectivity to ammonia, Eqs. (9) and (15), %
S_{N_2}	cycle-averaged selectivity to nitrogen, Eqs. (10) and (16), %
t_L	duration of the lean period, s
t_R	duration of the rich period, s
X_R	NO_x reduction conversion during the rich period, %

Subscripts

L	lean period
R	rich period

Superscripts

in	at the reactor inlet
out	at the reactor outlet

Greek symbols

ε_{NSR}	integral NSR efficiency, Eq. (17), %
η_T	NO_x trapping efficiency, Eq. (5), %
τ_L	dimensionless lean period relative to total cycle time
τ_R	dimensionless rich period relative to total cycle time

researches, such as different storage and reduction period, different reducing gas and different catalysts preparation and pretreatment [17,18]. In addition, the majority of the reports merely deals with one of the steps either storage or reduction and only a few contributions can be found trying to understand the behavior of the catalyst once a cycle-to-cycle steady-state has been established for the whole pseudo-real storage-reduction process.

Studying the link between storage and overall NO_x performance and reactor optimization is normally not a big issue in laboratory research reactor. It needs to be kept in mind that reaction engineering parameters such as gas hourly space velocity (GHSV), retention time, and lean/rich timing span strongly influence the overall performance of the NSR system. Kabin et al. [19] conducted an experimental study of NO_x storage and reduction on a series of model $Pt/BaO/Al_2O_3$ monolith catalysts to elucidate the relationship between the fraction of NO_x trapped (trapping efficiency) and reduced (time-average NO_x conversion), and to assess the dependence of catalyst performance on two key variables, the barium loading (6–25 wt% BaO) and space velocity (30,000–120,000 h^{-1}). They concluded that the dependence of the trapping efficiency on the exposure (storage) time provides a good estimate for the lean storage time needed to achieve a prescribed cycle-averaged NO_x conversion during cycling.

Recently, Clayton et al. [8] determined the effects of catalyst temperature, rich feed composition (NO, H_2, O_2), duration of the lean and rich steps, and the reductant to stored NO_x ratio on the cycle-averaged conversions and selectivities for a model $Pt/BaO/Al_2O_3$ lean NO_x trap using H_2 as the reductant. The cycle-averaged NO_x conversion exhibited a maximum at about 300 °C corresponding to the NO_x storage maximum. The N_2 selectivity exhibited a maximum at a somewhat higher temperature, at which point the NH_3 selectivity exhibited a minimum.

If NSR technology is to prove successful, the efficiency of the storage and reduction steps as well as the global NSR efficiency needs to be considered. The objective of this paper is to establish a definition for the integral efficiency of the NSR process, obviously related to the behavior of the catalyst, the mechanism of the NO_x storage phase and the kinetics of the NO_x release and reduction during the rich period. This definition should take into account the formation of any byproducts, resulting in improved NO_x-to-only N_2 reduction efficiency. The selectivity of the process strongly depends on the length of both lean and rich periods. Although there are numerous studies regarding long rich regeneration periods to investigate some mechanistic aspects of this phase [4,15,20], these may be unrealistic when applied to real lean-burn engines. In this sense, we have chosen a storage period in the range of some minutes, followed by rich spikes of several seconds. The effect of lean and rich period lengths, and reductant concentration is addressed and discussed in terms of the NO_x trapping efficiency in the lean period, NO_x reduction conversion in the rich period and selectivity to N_2/NH_3. The final goal is to propose a mathematical, graphical toolkit useful, based on the integral efficiency here defined, to compare the global NSR behavior of several commercial catalysts under almost real operating conditions.

2. Experimental

2.1. Catalyst preparation and characterization

A cordierite ($2MgO{\cdot}2Al_2O_3{\cdot}5SiO_2$) monolith, 20 mm in length and diameter, cut from a commercial sample supplied by Corning, with a cell density of 400 cells per square inch and a wall thickness of 150 μm was washcoated with γ-alumina supplied by Saint-Gobain (163 m^2 g^{-1}, after stabilization at 700 °C, 4 h). The washcoating was made by several immersions of the monolith in the alumina slurry until the desired amount of alumina was washcoated (≈500 mg).

The incorporation of platinum was carried out by adsorption from tetraamine platinum (II) nitrate solution supplied by Alpha Aesar and the excess of liquid remaining in the channels was blown out with compressed air. After calcination in air (500 °C, 4 h) and subsequent reduction of the metallic phase in a 5% H_2/N_2 stream (500 °C, 1 h), the barium was incorporated by immersion of the monolith in a barium acetate solution supplied by Aldrich. Finally, the catalyst was calcined again (500 °C, 4 h).

Specific details on the preparation and characterization of the $Pt–Ba/Al_2O_3$ monolith catalyst have been reported in our previous work [17]. The average Pt particle size was determined by H_2-chemisorption, resulting in 2.5 nm (Pt dispersion, 35%). The electron microscopy analysis of small amounts of washcoat scraped off from several zones of the monolith showed that the platinum particles were fairly well distributed on the entire sample surface, with most of crystallite particles sized around 1.3 nm. However, some larger particles (20 nm) were also observed in the powder scraped off just from the centre of the monolith, leading to the average Pt particle size of 2.5 nm determined by chemisorption. After barium incorporation, it was verified that there was no change in the Pt particle size. Concerning the barium phase, XRD measurements indicated that about 95% of Ba was uniformly dispersed on the surface. Platinum and barium loadings determined by ICP-MS resulted in 1.24 and 15.2 wt%, respectively.

2.2. NO_x storage-reduction measurements

The experiments were performed in a vertical down-flow stainless steel reactor. The reactor tube, with the monolith inside (3.52 g), was placed into a 3-zone tube furnace. Temperature was

Table 1
Experimental conditions used in experiments.

Operating parameter	Value(s)
Temperature (°C)	330
Total flow rate (slpm)	3.365
Lean period time (s)	145, 290, 595
Rich period time (s)	16–47
Lean gas composition	380 ppm NO, 6% O_2, balance N_2
Rich gas composition	380 ppm NO, 0.41–2.36% H_2, balance N_2

measured by thermocouples at the top and the bottom of the monolith. The reaction temperature was set for all experiments at 330 °C.

Table 1 shows the operational conditions used in the experiments. The composition of the lean gas mixture for NO_x storage was 380 ppm NO and 6% O_2 using N_2 as the balance gas. Gases were fed via mass flow controllers and the total flow rate was set at 3365 ml min^{-1}, which corresponded to a space velocity of 32,100 h^{-1} (standard conditions 25 °C, 1 atm). In order to find the efficient operating conditions to run the NSR process, three variables were studied: the duration of the lean period, the duration of the rich period and the reductant concentration during the regenerating period. Hydrogen was used as reductant and the concentration was varied from 0.41 to 2.36%. The duration of the lean and rich periods (t_L and t_R, respectively) was controlled by two solenoid valves which allowed precise definition of both cycles. The outlet gases concentration was continuously measured by using chemiluminiscence (NO_x), paramagnetic (O_2) and infrared (NH_3, N_2O) detectors (Rosemount Analytical).

To evaluate the performance of the catalyst during the lean and rich periods the NO_x trapping efficiency, NO_x conversion and N_2/NH_3 selectivities have been determined from the concentration curves at the reactor exit monitored during the experimental storage/reduction cycles.

(a) The total NO_x stored during the lean period, was calculated as

$$NO_x^{stored}(\mu mol\, NO_x) = (NO^{in})_L - (NO_x^{out})_L \quad (1)$$

where $(NO^{in})_L$ is the total amount of NO fed during the lean period and $(NO_x^{out})_L$ is the total amount of NO and NO_2 coming out from the reactor during the same period. These parameters can be calculated as follows:

$$(NO^{in})_L = F_{NO}^0 t_L \quad (2)$$

$$(NO_x^{out})_L = \int_0^{t_L} F_{NO_x}(t)dt \quad (3)$$

Consequently,

$$NO_x^{stored}(\mu mol\, NO_x) = F_{NO}^0 t_L - \int_0^{t_L} F_{NO_x}(t)dt = \int_0^{t_L} [F_{NO}^0 - F_{NO_x}(t)]dt \quad (4)$$

where F_{NO}^0 is the NO molar flow ($\mu mol\, min^{-1}$) at the reactor inlet, F_{NO_x} is the NO_x molar flow ($\mu mol\, min^{-1}$) at the reactor outlet and t_L (min) is the length of the lean period.

The outlet NO_x concentration was monitored as a function of time and then converted to the cumulative NO_x trapped as a percentage of the NO_x fed. This is referred to as the trapping efficiency (η_T) [19]:

$$\eta_T = \frac{NO_x^{stored}}{(NO^{in})_L} \times 100 = \frac{F_{NO}^0 t_L - \int_0^{t_L} F_{NO_x}(t)dt}{F_{NO}^0 t_L} \times 100 \quad (5)$$

(b) The NO_x reduction conversion (X_R) during the reduction period was calculated by

$$X_R(\%) = \frac{NO_x^{reduced}}{NO_x^{to\,be\,reduced}} = \frac{[NO_x^{stored} + (NO^{in})_R] - (NO_x^{out})_R}{[NO_x^{stored} + (NO^{in})_R]} \quad (6)$$

It is considered that the total amount of NO_x to be reduced accounts for the NO_x stored in the previous lean period plus the NO continuously added during the rich period $(NO^{in})_R$. On the other hand, $(NO_x^{out})_R$ refers to the amount of NO_x coming out from the reactor during the reduction period (t_R). Those amounts were calculated by

$$(NO^{in})_R = F_{NO}^0 t_R \quad (7)$$

$$(NO_x^{out})_R = \int_{t_L}^{t_L+t_R} F_{NO_x}(t)dt \quad (8)$$

(c) Selectivity to ammonia (S_{NH_3}) and nitrogen (S_{N_2}). Selectivity to ammonia is defined as the amount of NH_3 at the reactor outlet whenever was detected (mainly during the rich period and the first part of the subsequent lean period) related to the total amount of nitrogen containing products:

$$S_{NH_3} = \frac{NH_3^{out}}{NH_3^{out} + 2N_2^{out} + 2N_2O^{out}} \quad (9)$$

Similarly the selectivity to nitrogen can be defined as follows,

$$S_{N_2} = \frac{2N_2^{out}}{NH_3^{out} + 2N_2^{out} + 2N_2O^{out}} \quad (10)$$

Once a cycle-to-cycle steady-state is reached the nitrogen balance during the rich period can be expressed as

$$NO_x^{stored} + (NO^{in})_R = NH_3^{out} + 2N_2^{out} + 2N_2O^{out} + (NO_x^{out})_R \quad (11)$$

where

$$NH_3^{out} = \int_0^{t_L+t_R} F_{NH_3}(t)dt \quad (12)$$

$$N_2O^{out} = \int_0^{t_L+t_R} F_{N_2O}(t)dt \quad (13)$$

All experiments were conducted at 330 °C leading to a negligible formation of N_2O during the regeneration period; consequently, the N_2 production can be calculated from Eq. (11) as follows:

$$N_2^{out} = \tfrac{1}{2}[NO_x^{stored} + (NO^{in})_R - NH_3^{out} - (NO_x^{out})_R] \quad (14)$$

Substituting Eq. (14) into Eq. (9) and (10), taking into account the definition of X_R, Eq. (6) and after the adequate rearrangement, the following selectivity expressions can be deduced:

$$S_{NH_3} = \frac{NH_3^{out}}{X_R(NO_x^{stored} + (NO^{in})_R)} = \frac{\int_0^{t_L+t_R} F_{NH_3}(t)dt}{X_R\left(\int_0^{t_L}[F_{NO}^0 - F_{NO_x}(t)]dt + F_{NO}^0 t_R\right)} \quad (15)$$

$$S_{N_2} = \frac{2N_2^{out}}{X_R(NO_x^{stored} + (NO^{in})_R)} = \frac{\int_0^{t_L}[F_{NO}^0 - F_{NO_x}(t)]dt + F_{NO}^0 t_R - \int_0^{t_L+t_R} F_{NH_3}(t)dt - \int_{t_L}^{t_L+t_R} F_{NO_x}(t)dt}{X_R(\int_0^{t_L}[F_{NO}^0 - F_{NO_x}(t)]dt + F_{NO}^0 t_R)} \quad (16)$$

Eqs. (15) and (16) are similar to those previously used by Clayton et al. [8] to define the cycle-averaged NH_3 and N_2 selectivities when analyzing the performance of the NO_x trap over the total storage/reduction cycle.

(d) Integral NSR efficiency.

The parameters above defined allow us to compare independently the NO_x storage capacity during the lean period and the NO_x reduction conversion during the rich period. The N_2/NH_3 selectivities have been calculated averaged over the whole cycle, as peaks corresponding to those compounds can be seen at the outlet during the rich time but also continuing during the subsequent lean period (Fig. 1c later).

In the case of a conventional Pt–BaO/Al_2O_3NSR system, the catalyst should operate to exhibit high NO_x trapping efficiency with also high selectivity to N_2. Thus, the definition of a single parameter integrating the behavior of the trap over the whole storage/reduction cycle will be very useful to determine how to operate the NSR system in the most efficient way. This parameter should take into account the storage capacity, the reduction conversion and the selectivity of the reaction, giving a general vision of the efficiency of the NSR process, i.e. N_2 production related to the total amount of NO_x fed. Thus, the NSR efficiency is calculated by Eq. (17):

$$\varepsilon_{NSR} = \frac{2N_2^{out}}{(NO^{in})_L + (NO^{in})_R} = \frac{\int_0^{t_L}[F_{NO}^0 - F_{NO_x}(t)]dt + F_{NO}^0 t_R - \int_0^{t_L+t_R} F_{NH_3}(t)dt - \int_{t_L}^{t_L+t_R} R_{NO_x}(t)dt}{F_{NO}^0(t_L + t_R)} \quad (17)$$

3. Results and discussion

The physico-chemical characteristics of NSR monolith catalysts (Pt and Ba dispersion and distribution) are known to affect the catalytic behavior. As reported by Pereda-Ayo et al. [17] and Clayton et al. [21] the amount of stored NO_x increases with platinum dispersion. Furthermore, the Pt dispersion has a significant effect on the product distribution during the regeneration period. On the other hand, homogeneous distribution of barium increases the amount of storage sites available and also the interfacial area between Ba and Pt resulting in an improved NSR behavior [17]. However, the NO_x storage and reduction behavior is not only influenced by the physico-chemical characteristics of the catalyst, but also by the space velocity of reactants and temperature, as well as by tuning the operational conditions such as lean and rich period time and reductant concentration. In fact, the three variables t_L, t_R and C_{H_2} have been chosen as the parameters to be studied, while the temperature and space velocity were fixed at 330 °C and 32,100 h^{-1}. At such space velocity and temperature high trapping efficiencies are achieved as the NO oxidation approaches the equilibrium conversion limit [19].

Fig. 1 shows the effect of varying hydrogen concentration during the reduction period on the overall storage/reduction performance. These data and those that will be shown later were recorded after a steady cycle-to-cycle performance had been attained. In order to be closer to the real operation in the automobile converter, NO was continuously fed during lean and rich cycles. These cycles consisted of 145 s of storage (lean period) and 25 s of release/reduction (rich period). During the lean period the inlet gas mixture consisted of 6% O_2, 380 ppm NO and a balance of N_2. After 145 s, the oxygen was replaced by hydrogen for 25 s in the subsequent rich period. The evolution of oxygen concentration can be observed in Fig. 1a where a slight deviation from the ideal plug flow when shifting between lean and rich cycles can be noted [22]. Although oxygen was not fed during the rich cycle, the minimum concentration of

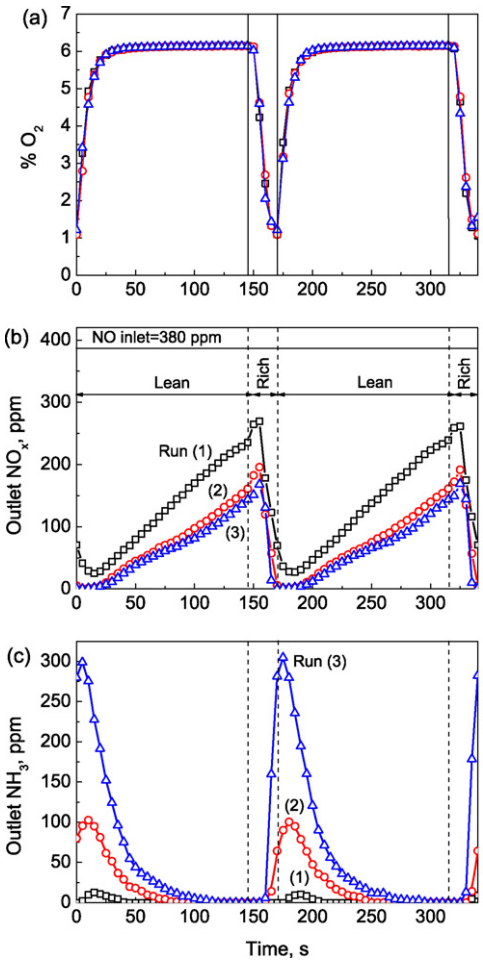

Fig. 1. Evolution of the outlet concentration of (a) oxygen, (b) NO_x and (c) NH_3 when using different hydrogen concentration during the rich period. Run (1) 0.79%, (2) 1.1% and (3) 2.32%.

this component was found to be around 1% at the end of the rich period, which means that the reduction process also occurred in the presence of some amount of oxygen. The NO_x storage and reduction performance with oxygen in the regeneration phase has been already studied by Epling et al. [23].

Fig. 1b shows the evolution of NO_x concentration at the reactor exit during the whole lean/rich cycle for three different hydrogen concentrations fed during the rich period, 0.79, 1.1 and 2.3% H_2. During the lean period the typical results were obtained, that is, the NO fed was stored in the catalyst decreasing the adsorption sites with time, and consequently increasing the NO_x outlet concentration. Proposed trapping mechanisms involve NO_2 formation on the Pt sites and then either subsequent diffusion via spillover type pathway to proximal trapping sites or gas phase transport to other trapping sites followed by nitrate formation via the disproportionation reaction [24–26]. As can be seen in Fig. 1b, none of the three experiments reached the NO_x inlet level (380 ppm) at the end of the lean period (145 s), just arriving to 240, 170 and 145 ppm NO_x in Runs 1, 2 and 3, respectively.

Previous studies have evidenced the influence of temperature during tests using Pt–BaO/Al_2O_3 catalysts. It has been reported by several authors that the largest amount of NO_x stored is generally observed at around 350 °C [27–30]. When the reaction temperature is increased above this optimum value the $Ba(NO_3)_2$ species formed during trapping become less stable reducing the NO_x storage capacity [29–31]. Muncrief et al. [29] also reported that the storage time, or saturation level, has an effect on the position of

the maximum storage capacity relative to temperature and, consequently, on the product distribution in the subsequent regeneration phase [12,15]. All the experiments in the present study were carried out at 330 °C, temperature at which maximum NO_x storage was recorded [32].

After 145 s of lean period, when the oxygen feed was replaced by hydrogen, a sudden release of the NO_x stored as nitrates/nitrites was observed due to the lower stability of these species when decreasing the oxygen partial pressure [15]. This behavior indicates that nitrate decomposition and release occur more rapidly than NO_x can be reduced [29]. Thus, in the first seconds of the rich period, a high local concentration of NO_x was recorded before reduction to N_2O, NH_3 or N_2. This concentration peak was more pronounced when a lower hydrogen concentration was used in the rich period.

During the regeneration period, the formation of N_2O and NH_3 was measured by our analysis system, whereas N_2 was calculated by the nitrogen balance, Eq. (14). Fig. 1c shows the ammonia detected at the reactor exit. Only traces of N_2O were detected (not shown). A peak concentration can be noticed for the three experiments described in this figure but with considerable different extent. It can also be noted that formation of ammonia was delayed with respect to the release of the stored NO_x as several authors have already reported [14,21,33–35]. The highest NH_3 outlet concentration was coincident in time with the lowest NO_x concentration. The NH_3 formed from the reaction between the released NO_x and H_2 continues to react further with the NO_x and is converted into N_2. Accordingly, in our experiments N_2 is supposed to be immediately formed at the reactor outlet and the NH_3 breakthrough is assumed to start after the hydrogen breakthrough, i.e. when the catalyst is becoming regenerated and stored nitrates are being depleted.

It is worth pointing out that 2.3% H_2 during the regeneration period led to the complete reduction of the gas phase NO_x (both released and fed during the regeneration period), Run (3) in Fig. 1b (CNO_x < 1 ppm). On the other hand, 0.79% H_2 was not able to achieve complete reduction in Run (1), with a NO_x outlet concentration around 25 ppm. The intermediate hydrogen concentration of 1.1% was found to be the lowest to achieve the complete NO_x reduction, Run (2). Such different regeneration performance affects not only the selectivity of the reaction but also the storage behavior in the subsequent cycle. The area between the inlet and the outlet NO_x concentration determined from Fig. 1b is related to the NO_x trapping efficiency (η_T), Eq. (5). In that sense, Fig. 1 reveals that theη_T increased with increasing the hydrogen concentration resulting in 40.8%, 77.3% and 80.5% for Runs (1), (2) and (3), respectively. Concerning ammonia production, notable differences can be noticed in Fig. 1c. The highest ammonia concentration was 300, 100 and 10 ppm when 2.3, 1.1 and 0.79% H_2 was fed during the regeneration, respectively. Thus, a higher hydrogen concentration led to the formation of a larger amount of ammonia. This trend was expected according to previous studies [10,15,16,35,36].

In order to gain insight into the way hydrogen concentration during the rich period influences the amount of NO_x stored and N_2/NH_3 selectivity, a set of experiments was performed with intermediate H_2 concentrations. From the NO_x storage/reduction profiles similar to those included in Fig. 1b, the NO_x trapping efficiency (η_T), the reduction conversion (X_R) and the selectivity to nitrogen (S_{N_2}) were calculated by Eq. (5), (6) and (16), respectively. The evolution of these parameters with H_2 concentration is shown in Fig. 2a (Fig. 2b and c will be discussed later). Up to 1.1% H_2 the η_T sharply increased, whereas from 1.1% H_2 and above it was hardly influenced by the addition of more reductant.

Clayton et al. [21] proposed a schematic diagram showing the different storage regions related to the barium phase storage sites based on their proximity to Pt crystallites. These authors defined the "proximal region" with barium storage sites that are located close to the Pt–BaO interface and participate actively in the storage

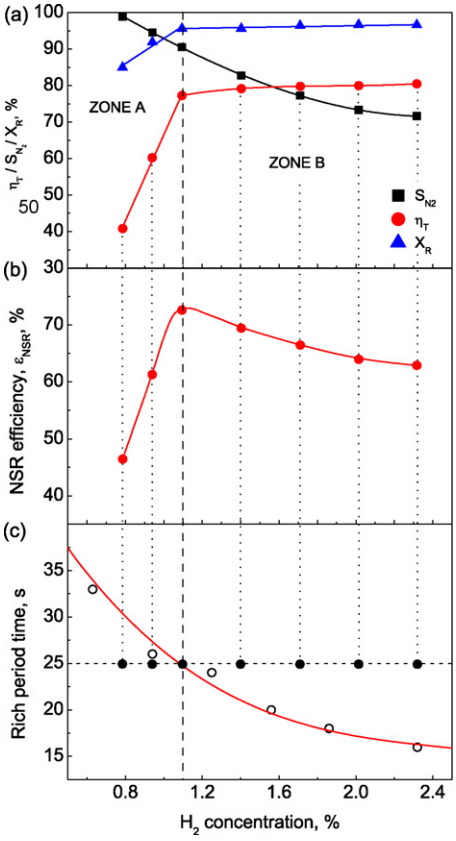

Fig. 2. Analysis and relation between variables describing the catalytic performance (a). Calculated NO_x trapping efficiency, conversion reduction and selectivity to nitrogen with hydrogen concentration for t_L = 145 s and t_R = 25 s, (b) NSR efficiency, and (c) operational variables (C_{H_2}, t_R) to run the NSR process efficiently for a given t_L of 145 s.

and reduction of NO_x. The "regenerated region" comprises storage sites that are regenerated during the NO_x reduction step. In contrast, storage sites in the "bulk region", i.e. BaO sites further removed from the Pt and also BaO sites beneath the surface, do not play a key role in the storage process once a cyclic steady-state is reached. They associated the extension of these regions with the platinum dispersion and the reaction temperature. From our results, we can suggest that the extension of the regenerated region also depends on the H_2 concentration fed during the reduction period, i.e. a higher H_2 concentration regenerates more storage sites during the NO_x reduction step. This makes possible to expand the regenerated area, with the corresponding increase in the NO_x trapping efficiency as shown in Fig. 2a, up to 1.1% H_2. For hydrogen concentration above 1.1%our experiments showed that nearly the same NO_x trapping efficiency was attained, probably due to the complete regeneration of the catalyst surface has already been achieved.

Fig. 2a shows a similar trend for the reduction conversion, although less pronounced. Above 1.1% H_2 almost total NO_x conversion was achieved (≈97%), whereas this conversion was lower when the hydrogen concentration was set below 1.1% H_2. With lower hydrogen concentrations a higher fraction of the stored NO_x was released without being reduced during the reduction period as reveals the higher concentration of NO_x recorded at the beginning of the rich cycle (Fig. 1b). In fact, for 0.79% H_2 the NO_x reduction conversion decreased to 85%.

The maximum NH_3 outlet concentration decreased when decreasing the hydrogen concentration fed in the rich period, approaching zero for 0.79% H_2, which corresponds to near 100% nitrogen selectivity (Run (1) in Fig. 1c). This evolution of the product

distribution can be explained in terms of the H_2/NO_x ratio during the reduction period, as Clayton et al. [8] have already reported. When the H_2/NO_x ratio decreases, i.e. lower hydrogen concentration is fed, nitrogen is the primary product of the reduction, whereas for higher H_2/NO_x ratios the ammonia formation is promoted.

Two different zones can be clearly distinguished in Fig. 2a, zone A (below 1.1% H_2) and zone B (above 1.1% H_2). In the zone A, hydrogen was the limiting reactant in the release/reduction step and the complete reduction of NO_x was not achieved (as shown in the NO_x storage-reduction profile for 0.79% H_2, Run (1) in Fig. 1b). In the zone B, the reaction occurred with excess of hydrogen resulting in the complete reduction of NO_x (Run 3 in Fig. 1b). Moreover, this differentiated NO_x reduction profile has a significant importance for the efficiency of the NSR process. If the reaction is carried out under regenerating conditions corresponding to the zone A, H_2 is in defect and total reduction of gas phase NO_x is not achieved, leading to a low NO_x trapping efficiency after the steady-state is reached. In contrast, regenerating conditions in zone B supply H_2 in excess, favoring the production of ammonia instead of nitrogen.

At this point, we suggest introducing a new parameter to provide a general vision of the efficiency of the NSR process, namely ε_{NSR}, defined as the N_2 production related to the total amount of NO_x entering the trap, and calculated by Eq. (17). The evolution of ε_{NSR} with hydrogen concentration is described in Fig. 2b. The NSR efficiency takes into account jointly the NO_x trapping efficiency, the reduction conversion and the selectivity of the reaction. In that sense, although practically total selectivity to nitrogen is obtained for low H_2 concentration, the NSR efficiency is poor due to the low values of the NO_x trapping efficiency and reduction conversion. On the other hand, high H_2 concentration allows to obtain the maximum NO_x trapping efficiency and reduction conversion but with considerable ammonia generation, resulting again in a decrease in the NSR efficiency relative to the maximum. The limit between the zones A and B, corresponding to 1.1% H_2, is suitable for a good compromise among NO_x trapping efficiency, conversion and selectivity, resulting in the maximum of NSR efficiency (70%), which means that 70% of NO_x fed to the reactor is converted into N_2.

As we have previously reported, 1.1% H_2 was found to be also the minimum hydrogen concentration to attain total reduction of the released and fed NO_x (Fig. 1b, Run (2)) for a given lean and rich period time of 145 and 25 s, respectively. In that sense, a relationship between the reduction profile and the NSR efficiency can be established, that is, the regenerating conditions which achieve total reduction of NO_x by supplying the adequate amount of hydrogen (neither in defect nor in excess) thereby maximizing the NSR efficiency.

Up to now the analysis has been carried out with the fixed values of the storage and regeneration periods (t_L = 145 s and t_R = 25 s). Next, we will present new experiments to examine the influence of the duration of the storage and regeneration periods on the behavior of the catalyst, as the optimal hydrogen concentration to achieve the most efficient operation may result altered.

First, several NO_x storage/reduction cycles were run varying the hydrogen concentration from 0.41 to 2.32% (Table 2, first section), for a given lean period of 145 s. For each hydrogen concentration the shortest rich period to obtain total reduction of NO_x was experimentally determined, as to fit the above stated requirement for the most efficient operation. Fig. 3 shows the outlet NO_x and ammonia concentration profiles when 2.32, 1.25 and 0.41% H_2 was used during the rich period. The end of the rich period was experimentally established once the NO_x outlet concentration was reduced to practically zero, afterwards beginning the next lean period. Several consecutive cycles were run until the steady cycle-to-cycle performance was attained. As expected, Fig. 3 reveals that the lower hydrogen concentration, the longer rich period was needed to obtain complete reduction, i.e. 16 s (Fig. 3a), 24 s (Fig. 3b) and 41 s (Fig. 3c) for 2.32, 1.25 and 0.41% H_2, respectively. In contrast, the evolution of the outlet ammonia concentration was practically identical, with the NH_3 breakthrough taking place in the last seconds of the rich period and extended to the first part of the subsequent lean period. Moreover, the area under the outlet NH_3 concentration resulted in very similar values irrespective of theH_2 concentration and rich period length combination (C_{H_2}, t_R), which means that the same selectivity to N_2 (≈91%) was achieved in the three experiments represented in Fig. 3. It can also be seen that the evolution of the outlet NO_x concentration during the 145-s long lean period was exactly the same for the three described situations, which thus corresponds to a NO_x trapping efficiency of 77%. Overall, various combinations (C_{H_2}, t_R) can be found to operate the rich period making the NSR process efficient. Furthermore, these different combinations (C_{H_2}, t_R) led to the same NO_x trap-

Table 2
Calculated response variables, NO_x trapping efficiency, reduction conversion, selectivity to nitrogen and NSR efficiency as a function of the operational variables (C_{H_2}, t_R, t_L).

t_R (s)	C_{H_2} (%)	$(NO^{in})_R$ (μmol)	$(NO_x^{out})_L$ (μmol)	$(NO_x^{out})_R$ (μmol)	(NO_x^{stored}) (μmol)	NH_3^{out} (μmol)	N_2^{out} (μmol)	η_T (%)	X_R (%)	S_{N_2} (%)	ε_{NSR} (%)
t_L = 145 s, $(NO^{in})_L$ = 113.2 μmol											
16	2.32	12.5	25.4	4.2	87.8	9.8	86.3	77.6	95.8	89.8	68.7
18	1.86	14.0	25.3	4.3	87.9	9.5	88.1	77.7	95.8	90.3	69.3
20	1.56	15.6	25.6	5.0	87.6	8.6	89.6	77.4	95.2	91.2	69.6
24	1.25	18.7	25.6	5.2	87.6	10.2	90.9	77.4	95.1	89.9	68.9
26	0.94	20.3	25.9	6.1	87.3	8.2	93.3	77.1	94.3	91.9	69.9
33	0.63	25.7	25.6	8.4	87.6	8.6	96.3	77.4	92.6	91.8	69.3
41	0.41	32.0	25.7	10.0	87.5	9.6	99.9	77.3	91.6	91.2	68.8
t_L = 290 s, $(NO^{in})_L$ = 226.3 μmol											
25	2.32	19.5	101.5	7.4	124.8	13.9	123.4	55.1	95.1	89.9	50.2
26	1.86	20.3	100.9	7.9	125.4	12.9	124.9	55.4	94.6	90.6	50.6
28	1.56	21.8	100.4	8.4	125.9	10.9	128.4	55.6	94.3	92.2	51.8
31	1.25	24.2	101.8	9.0	124.5	11.7	128.0	55.0	93.9	91.6	51.1
35	0.94	27.3	101.3	10.0	125.0	10.5	131.8	55.2	93.4	92.6	52.0
39	0.78	30.4	101.7	11.0	124.6	12.5	131.5	55.1	92.9	91.3	51.2
46	0.63	35.9	101.5	12.3	124.8	11.4	137.0	55.1	92.3	92.3	52.2
t_L = 595 s, $(NO^{in})_L$ = 464.4 μmol											
32	2.32	25.0	302.0	5.0	162.4	24.5	157.9	35.0	97.3	86.6	32.3
35	1.86	27.3	301.4	5.5	163.0	26.7	158.1	35.1	97.1	85.6	32.2
38	1.56	29.6	301.6	6.2	162.8	25.5	160.7	35.1	96.8	86.3	32.5
42	1.25	32.8	302.0	7.0	162.4	25.8	162.4	35.0	96.4	86.3	32.7
47	1.09	36.7	302.4	8.9	162.0	24.1	165.7	34.9	95.5	87.3	33.1

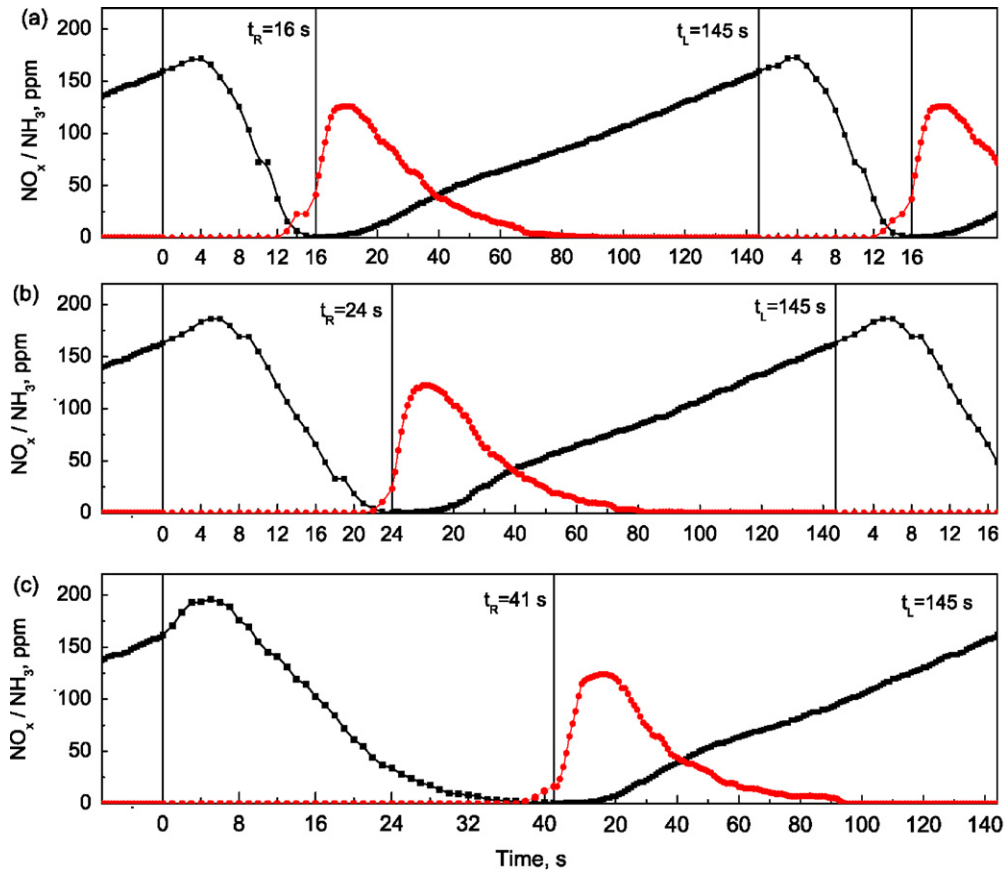

Fig. 3. Evolution of the outlet NO_x and NH_3 concentration with time for different hydrogen concentration (a) 2.32% H_2 (b) 1.25% H_2 (c) 0.41% H_2. The rich period duration was adjusted to achieve total NO_x reduction.

ping efficiency as can be seen in the ninth column of Table 2 (first section), also expected because the outlet NO_x curve during the lean period resulted invariable. Selectivity to nitrogen and NSR efficiency resulted in very comparable values as well. The locus of all these combinations is shown in Fig. 2c (empty symbols) and represents the isocurve of operational conditions to carry out the integral NSR process efficiently.

It is worth noting some deviation in the total amount of hydrogen fed during the rich period between different experiments on the isocurve. The effect of an increase in the amount ($C_{H_2} \times t_R$) with decreasing t_R is primarily a result of the axial mixture deviation from the ideal plug flow during the lean-rich transition. As reported elsewhere [22], reducing the rich period length resulted in an increasing contribution of the H_2–O_2 reaction due to rich-to-lean and lean-to-rich transitions. In addition, the reaction between the residual oxygen present in the rich period and the hydrogen fed is also responsible for needing an amount of reductant ($C_{H_2} \times t_R$) higher than the stoichiometric for reducing the NO_x fed and released (Table 2).

The shape of the isocurve represented in Fig. 2c indicates the inverse relationship between the reduction time and the reductant concentration to achieve an efficient NSR process, i.e. the shorter reduction time, the higher reductant concentration. This finding implies that the supply of the reductant H_2 is controlling the NSR process. This was also observed by Mulla et al. [14] that measured the time required for regenerate the trap catalyst by the width of the N_2 pulse in a mass spectrometer. Analogously, Nova et al. [33] had also noticed that the N_2 production during the regeneration of a Pt–BaO/Al_2O_3 catalyst is limited by the amount of H_2 fed to the reactor.

The analysis of the relationship among representations in Fig. 2a–c can help to understand the term "efficient operation" that we have used above. All runs in Fig. 2a and b correspond to a regeneration time of 25 s, which is the horizontal line in Fig. 2c. It can be seen that the efficient operation point, as defined in Fig. 2b, corresponds to the only point on the isocurve in Fig. 2c for t_R = 25 s. For a given combination of rich period time and hydrogen concentration (C_{H_2}, t_R) above the isocurve (e.g. all points on the right of the horizontal line, for t_R = 25 s) the operation is carried out under conditions of zone B in Fig. 2a where the NO_x trapping efficiency is maintained at higher values but with a lower selectivity to N_2 due to the excess of hydrogen in the environment during the regeneration. This fact makes the operation in this zone inefficient and thus not recommendable for real application. On the contrary, below the isocurve (to the left of the horizontal line, for t_R = 25 s) the operation occurs under conditions of zone A (Fig. 2a) where there is not enough supply of hydrogen for complete regeneration leading to a significant reduction in the NO_x trapping efficiency with high selectivity to N_2. In conclusion, only when operating at points situated on the isocurve the adequate amount of H_2 will be supplied resulting in the operation mode that we are suggesting as the "most efficient" for real application, with sufficiently high level of both the storage capacity and selectivity to nitrogen.

To further investigate the optimal conditions to operate the NSR process efficiently, the duration of the storage period was also varied, extending the lean period length from 145 to 290 and 595 s. Again, analogous NO_x storage and reduction experiments were performed with those extended times and the same protocol as before. The minimum duration of the rich period needed to obtain the complete reduction of NO_x was experimentally determined for each

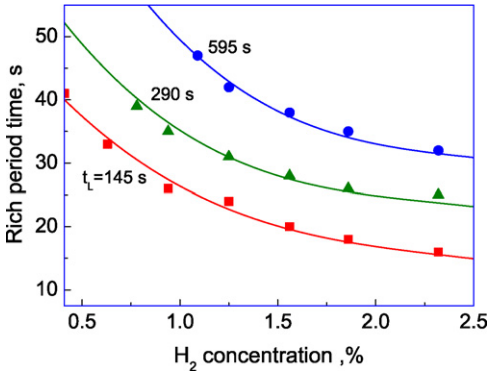

Fig. 4. Operation map of the prepared catalyst. Relation of the operational variables (C_{H_2}, t_R, t_L) to run the NSR process efficiently.

selected H_2 concentration. Sections 2 and 3 of Table 2 include the different combinations (C_{H_2}, t_R) found as to fit the requirements for efficient operation for t_L = 290 and 595 s, respectively. As before, it has been verified that the same trapping efficiency was obtained for a given lean period duration, resulting in additional isocurves shown in Fig. 4. The NO_x trapping efficiency η_T, reduction conversion (X_R), selectivity (S_{N_2}) and NSR efficiency (ε_{NSR}) are shown in Sections 2 and 3 of Table 2 for t_L = 290 and 595 s, respectively. As expected, the NO_x trapping efficiency decreased as the lean period duration increased. When the lean period is longer the catalyst is closer to the saturation level, and consequently the trapping efficiency decreases, i.e. 77, 55 and 35% for t_L = 145, 290 and 595 s, respectively. As for selectivity to nitrogen, very similar values were found around 90%, irrespective of the studied variables (C_{H_2}, t_R, t_L) provided that the operation is conducted at efficient conditions (all points in Fig. 4).

As noted above, the nitrogen production during the regeneration of the catalyst is limited by the amount of hydrogen fed to the reactor. Likewise, increasing the hydrogen supply rate is expected to have a linear effect on the overall rate of NO_x reduction. For our experiments, Fig. 5 shows a linear effect of the hydrogen concentration fed during the rich period on the overall NO_x reduction rate, independent of the duration of the lean period, also suggesting that the regeneration step is limited by the amount of hydrogen fed. The linear relationship implies that the time required for complete regeneration should be inversely proportional to the reductant amount of hydrogen fed, as shown in the isocurves from Fig. 4. Mulla et al. [14] also reported the overall rate for NO_x reduction as a linear function of rate of flow of H-atoms in the form of H_2 or NH_3 at 300 °C. Their observations also confirmed that the regeneration process was not mass transfer

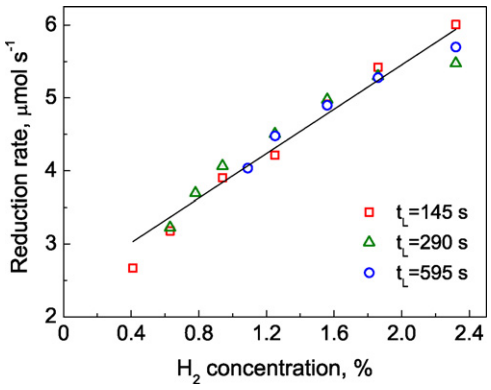

Fig. 5. Linear relation between overall NO_x reduction rate versus hydrogen concentration.

or kinetically limited, but it was controlled by the supply of the reductant H_2.

Finally, we can suggest the term "operation map" for the set of curves represented in Fig. 4, as to find any combination of the three studied operational variables – the duration of the lean period, the duration of the rich period and the concentration of the reducing agent – to run the NSR process efficiently. Two ideas may arise from this map. First, every manufactured catalyst can be associated with its own map, so that the comparison of maps will provide information about their relative efficiency when running under the real application. Secondly, one may wonder if any operation point in the map of Fig. 4 is susceptible to be chosen as the best combination (C_{H_2}, t_R, t_L) to run in real application.

The best NSR efficiency corresponds to points in the first section of Table 2, where the duration of the lean period has been given as 145 s. Any combination (C_{H_2}, t_R) in that section gives $\varepsilon_{NSR} \approx 69\%$. However, when a higher reductant concentration is used the responsiveness in t_R is low as deduced from the flatness of the isocurve in that region. Therefore (C_{H_2}, t_R) = (2.32%, 16 s) can be chosen as the best operational conditions leading to the following outputs of the process:

$$\eta_T = 77.6\%; \qquad X_R = 95.9\%; \qquad S_{N_2} = 89.8\%; \qquad \varepsilon_{NSR} = 68.7\%$$

Throughout the paper various response variables namely η_T, X_R and S_{N_2} have been defined to describe the kinetic behavior of the catalyst with the aim of determining the operational conditions t_L, t_R and C_{H_2} which allow running the NSR process in the most efficient way. This behavior has been suggested to be described with the only variable defined as the NSR efficiency (ε_{NSR}). Combination and rearrangement of Eq. (5), (6), (16) and (17) allows to relate the NSR efficiency with the other variables describing independently the behavior of the storage and reduction phases, resulting in

$$\varepsilon_{NSR} = X_R S_{N_2} [\eta_T \tau_L + \tau_R] \tag{18}$$

where τ_L and τ_R are dimensionless lean and rich times relative to the total time of the whole cycle,

$$\tau_L = \frac{t_L}{t_L + t_R}; \qquad \tau_R = \frac{t_R}{t_L + t_R} \tag{19}$$

Eq. (18) can be easily verified from comparison of values given in the last (twelfth) column of Table 2, and those calculated from ninth, tenth and eleventh columns.

4. Conclusions

The NO_x storage and reduction performance is strongly affected by operating conditions such as the length of the storage and reduction periods, and the reductant concentration. The influence of these variables on the catalytic behavior has been widely studied in this paper.

First, the attention was focused on the influence of the reductant concentration. For fixed lean and rich periods of 145 and 25 s, respectively, we found that 1.1% H_2 was the minimum concentration needed to obtain complete reduction of gas phase NO_x, both released and fed during the regeneration. Varying hydrogen concentration affected not only the reduction pattern and selectivity but also the behavior during the storage period. Consequently, the evaluation of the NSR activity has to be made for the whole process taking into account both the storage and the reduction periods. Thus, we have proposed the new parameter ε_{NSR}, which gives a general vision of the efficiency of the NSR process, defined as the moles of N_2 at the reactor outlet related to the total amount of NO_x entering the trap, expressed as percentage. We have verified that the minimum hydrogen concentration to obtain total NO_x reduction during regeneration (1.1% H_2), experimentally determined, also corresponded to the highest NSR efficiency, around

70%. A higher H_2 concentration favored the ammonia production at the cost of decreasing the selectivity to nitrogen, and a lower H_2 concentration impacted negatively on the storage due to an incomplete regeneration. None of those achieved efficiency as high as 70%.

Secondly, the variation of the reduction period length was analyzed. An inverse relationship between the reduction time, t_R and reductant concentration, C_{H_2}, to obtain complete NO_x reduction was deduced. We found different combinations of both operating variables (C_{H_2}, t_R) which led to the same selectivity, and also to the same storage capacity. The locus of those combinations defines the iso-efficiency curve to run the NSR more efficiently (70%) with a good balance between the storage capacity and the selectivity to nitrogen.

To further investigate the optimal conditions to operate efficiently the NSR process, the duration of the storage period was also modified. When extending the lean period time, the NO_x trapping efficiency decreased but a higher amount of NO_x was stored in the catalyst. Consequently, for longer storage periods the operating conditions (C_{H_2}, t_R) during the reduction period were altered, and the ε_{NSR}-isocurve was shifted to lower values of the maximum efficiency, i.e. when t_L = 290 s $(\varepsilon_{NSR})_{max}$ = 51%, and for t_L = 595 s $(\varepsilon_{NSR})_{max}$ = 32%.

The family of ε_{NSR}-isocurves represents the maximum efficiency that can be achieved for different combinations of the three studied operational variables (C_{H_2}, t_R, t_L). We have suggested the term "operation map" for this graph. Analysis of the operation maps corresponding to different catalysts will allow to predict the NSR behavior and to compare their efficiency for a given set of operational conditions.

Although the space velocity and temperature have been maintained in 32,100 h^{-1} and 330 °C for all experiments reported here, these results help to determine how to operate the integral NSR process in the most efficient way, to exhibit high NO_x trapping efficiency and high selectivity to N_2 in the conventional lean NO_x traps. Ongoing studies carried out in our laboratory include experimenting other space velocities and temperatures.

Acknowledgements

The authors wish to acknowledge the financial support provided by the Spanish Science and Innovation Ministry (CTQ2006-15079 and CTQ2009-12517), the Basque Government (Consolidated Research Group, GIC 07/67-JT-450-07) and the Regional Government of Bizkaia (DIPE 07/11). One of the authors (BPA) wants to acknowledge to the Spanish Science and Innovation Ministry for the PhD Research Grant.

References

[1] N. Miyoshi, S. Matsumoto, T. Katoh, T. Tanaka, J. Harada, N. Takahashi, K. Yokota, M. Sugiara, K. Kasahara, SAE Techn. Pap. 950809 (1995).
[2] N. Takahashi, H. Shinjoh, T. Iijima, T. Suzuki, K. Yamazaki, K. Yokota, H. Suzuki, N. Miyoshi, S. Matsumoto, T. Tanizawa, T. Tanaka, S. Tateishi, K. Kasahara, Catal. Today 27 (1996) 63.
[3] W.S. Epling, L.E. Campbell, A. Yezerets, N.W. Currier, J.E. Parks, Catal. Rev. Sci. Eng. 46 (2004) 163.
[4] H. Abdulhamid, E. Fridell, M. Skoglundh, Top. Catal. 30–31 (2004) 161.
[5] Z. Liu, J.A. Anderson, J. Catal. 224 (2004) 18.
[6] H. Abdulhamid, J. Dawoody, E. Fridell, M. Skoglund, J. Catal. 244 (2006) 169.
[7] J. Theis, H-W. Jen, R. McCabe, M. Sharma, V. Balakotaiah, M.P. Harold, SAE Techn. Pap. Series 2006-01-1067 (2006).
[8] R.D. Clayton, M.P. Harold, V. Balakotaiah, AIChE J. 55 (2009) 687.
[9] S. Roy, A. Baiker, Chem. Rev. 109 (2009) 4054.
[10] A. Lindholm, N.W. Currier, E. Fridell, A. Yezerets, L. Olsson, Appl. Catal. B: Environ. 75 (2007) 78.
[11] F. Prinetto, G. Ghiotti, I. Nova, L. Lietti, E. Tronconi, P. Forzatti, J. Phys. Chem. B 105 (2001) 12732.
[12] R.D. Clayton, M.P. Harold, V. Balakotaiah, Appl. Catal. B: Environ. 84 (2008) 616.
[13] H. Abdulhamid, E. Fridell, M. Skoglundh, Appl. Catal. B: Environ. 62 (2006) 319.
[14] S.S. Mulla, S.S. Chaugule, A. Yezerets, N.W. Currier, W.N. Delgass, F.H. Ribeiro, Catal. Today 136 (2008) 136.
[15] W.S. Epling, A. Yezerets, N.W. Currier, Appl. Catal. B: Environ. 74 (2007) 117.
[16] I. Nova, L. Castoldi, L. Lietti, E. Tronconi, P. Forzatti, Top. Catal. 42–43 (2007) 21.
[17] B. Pereda-Ayo, R. López-Fonseca, J.R. González-Velasco, Appl. Catal. A: Gen. 363 (2009) 73.
[18] B. Pereda-Ayo, D. Divakar, R. López-Fonseca, J.R. González-Velasco, Catal. Today 147 (2009) S244.
[19] K.S. Kabin, R.L. Muncrief, M.P. Harold, Y. Li, Chem. Eng. Sci. 59 (2004) 5319.
[20] A. Amberntsson, E. Fridell, M. Skoglundh, Appl. Catal. B: Environ. 46 (2003) 429.
[21] R.D. Clayton, M.P. Harold, V. Balakotaiah, C.Z. Wan, Appl. Catal. B: Environ. 90 (2009) 662.
[22] U. Elizundia, R. López-Fonseca, M.A. Gutiérrez-Ortiz, J.R. González-Velasco, Chem. Eng. J. 150 (2009) 447.
[23] W.S. Epling, D. Kisinger, C. Everest, Catal. Today 136 (2008) 156.
[24] J.H. Kwak, D.H. Kim, T. Szailer, C.H.F. Peden, J. Szanyi, Catal. Lett. 111 (2006) 119.
[25] I. Nova, L. Lietti, L. Castoldi, E. Tronconi, P. Forzatti, J. Catal. 239 (2006) 244.
[26] W.S. Epling, J.E. Parks, G.C. Campbell, A. Yezerets, N.W. Currier, L.E. Campbell, Catal. Today 96 (2004) 21.
[27] L. Lietti, P. Forzatti, I. Nova, E. Tronconi, J. Catal. 204 (2001) 175.
[28] H. Mahzoul, J.F. Brilhac, P. Gilot, Appl. Catal. B: Environ. 20 (1999) 47.
[29] R.L. Muncrief, P. Khanna, K.S. Kabin, M.P. Harold, Catal. Today 98 (2004) 393.
[30] K.S. Kabin, R.L. Muncrief, M.P. Harold, Catal. Today 96 (2004) 79.
[31] E. Fridell, M. Skoglundh, B. Westerberg, S. Johansson, G. Smedler, J. Catal. 183 (1999) 196.
[32] B. Pereda Ayo, J.J. Delgado, R. López-Fonseca, J.J. Calvino, S. Bernal, J.R. González-Velasco, Annual AIChE Meeting, Pennsylvania, Philadelphia, November 2008.
[33] I. Nova, L. Lietti, P. Forzatti, Catal. Today 136 (2008) 128.
[34] L. Lietti, I. Nova, P. Forzatti, J. Catal. 257 (2008) 270.
[35] L. Cumaranatunge, S.S. Mulla, A. Yezerets, N.W. Currier, W.N. Delgass, F.H. Ribeiro, J. Catal. 246 (2007) 29.
[36] J. Pihl, J. Parks, S. Daw, T. Root, SAE Techn. Pap. Series 2006-01-3441 (2006).